Ion Dynamics in Steady Collisionless Driven Reconnection

Wenbing Pei,[1] Ritoku Horiuchi,[1,2] and Tetsuya Sato[1,2]
[1]*The Graduate University for Advanced Studies, Oroshi-cho 322-6, Toki, 509-5292, Japan*
[2]*Theory and Computer Simulation Center, National Institute for Fusion Science, Oroshi-cho 322-6, Toki, 509-5292, Japan*
(Received 26 March 2001; published 16 November 2001)

Steady collisionless driven reconnection in an open system is investigated by means of a new two-dimensional full-particle simulation. The reconnection rate is controlled by an external driving electric field. Ion-meandering motion plays an important role in ion dynamics which controls the spatial structures of ion quantities. Although the electric current is predominantly carried by electrons, the current layer has the half-width of the ion-meandering orbit scale because the density profile is controlled by massive-ion motion. Thus, the global dynamic behavior of reconnection is dominantly controlled by ion dynamics. An electrostatic field generated through the finite-Larmor-radius effect leads to electron acceleration in the equilibrium current direction in the ion-dissipation region and ion heating by intensifying meandering motion. Our results are in agreement with the recent experimental results of Yamada *et al.* [Phys. Plasmas **7**, 1781 (2000)] and of Hus *et al.* [Phys. Rev. Lett. **84**, 3859 (2000)].

DOI: 10.1103/PhysRevLett.87.235003 PACS numbers: 52.35.Qz, 52.65.Rr, 94.30.Ej

Collisionless magnetic reconnection plays a crucial role in a number of interesting phenomena with fast magnetic energy release and plasma acceleration and heating both in space plasmas [1,2] and in laboratory plasmas [3–5]. Although recent studies from laboratory plasma experiments, satellite observations, theoretical analysis, and computer simulations have advanced the understanding of magnetic reconnection, the fundamental physics of fast reconnection remains unknown until today. Many studies of collisionless reconnection focus on the understanding of the reconnection mechanism, in particular, reconnection rate, dissipation region size, current layer width, and their relation with electron and ion dynamics. Recent numerical studies of nondriven reconnection in a closed system indicate that the reconnection rate is controlled by the ion dynamics based on the Hall effect which is faster than on the resistivity, and is essentially independent of the electron dynamics [6–8]. The corresponding current layer width is, however, scaled by the electron skin depth δ_e ($= c/\omega_{pe}$) or Larmor radius ρ_e [8]. On the other hand, experimental studies in the Magnetic Reconnection Experiment (MRX) have found that the current layer width is about $0.4\delta_i \sim \rho_i$ [4] and the significant nonclassical ion heating occurs [4,5], where $\delta_i = c/\omega_{pi}$ is the ion collisionless skin depth and ρ_i is the ion Larmor radius.

Collisionless reconnection driven by an external plasma inflow, namely collisionless driven reconnection, is one of the potential candidates for fast reconnection because the reconnection rate is mainly controlled by the external driving conditions [9]. Horiuchi and Sato [10,11] have performed the particle simulation of collisionless driven reconnection and found that the reconnection electric field evolves in two steps in accordance with the formation of ion and electron current layers, but the global evolution is exclusively controlled by the ion dynamics. However, their studies are limited to a relatively early phase because a periodic condition is used at the downstream boundary. We have extended the previous model [11] to an open system and investigated long time scale evolution of collisionless driven reconnection. It is found that the temporal behavior of reconnection depends strongly on the uniformity of the external driving inflow. As the nonuniformity scale increases, the reconnection evolution transits from a steady regime into an intermittent regime. In this Letter, our focus is on the physical mechanism of steady reconnection. The transition mechanism will be discussed elsewhere [12].

A new two-and-a-half-dimensional explicit electromagnetic particle simulation code for an open system is developed based on the previous version [11]. The simulation is performed in the x-y plane. At the upstream boundary ($y = \pm y_b$), the plasma inflow is driven by an external electric field imposed in the opposite z direction. The other condition is taken as $E_x = 0$. The downstream boundary ($x = \pm x_b$) is free, across which plasma can freely flow in or out. The downstream boundary conditions for field quantities assume that E_y and $\partial_x E_z$ are continuous. As to the boundary conditions for particles, the net number of particles passing the boundary during one time step is determined by calculating the plasma outflow, and thereby some particles are reinserted according to the charge neutrality condition [13].

The simulation begins with a Harris-type equilibrium as $B_x(y) = B_0 \tanh(y/L)$, where B_0 is a constant and L is the scale height along the y axis. The initial particle distribution is a shifted Maxwellian with a spatially uniform temperature and the average particle velocity which is equal to the diamagnetic drift velocity. The simulation is carried out on a 512×128 point grid by making use of 6.4 million particles. The main parameters are the following: the mass ratio of ion to electron $m_i/m_e = 25$, $T_{i0}/T_{e0} = 1$, $\omega_{pe0}/\omega_{ce0} = 3.5$, and $L = 0.8y_b \approx 3\rho_{i0}$, where ω_{pe0} is the plasma frequency, ω_{ce0} is the electron cyclotron frequency associated with B_0, and ρ_{i0} is the ion Larmor radius. The time step is chosen as $\omega_{ce0}\Delta t = 0.02$.

The external driving electric field $E_{zd}(x,t)$ imposed at the upstream boundary at five different times is shown in Fig. 1 where λ_{d0} is the Debye length. After $\omega_{ci0}t = 5.72$, E_{zd} keeps a constant E_0 which is a necessary condition for steady reconnection. Another key parameter characterizing E_{zd} is the early-phase nonuniformity scale x_d. Although E_{zd} is uniform in the later time, the magnetic field at the upstream boundary is always nonuniform, and depends strongly on x_d. In other words, the nonuniformity scale x_d affects the shape of magnetic field lines at the input boundary, and thus the pattern of plasma inflow.

The steady magnetic reconnection is realized in six simulation runs with the sets of $E_0/B_0 = -0.04, -0.06, -0.08$ and $x_d/x_b = 0.42, 0.62$, in which there is only one stable X point located near the center of the simulation domain (the coordinate origin) [12]. All the runs exhibit the identical characteristics. The following discussion on the features of steady reconnection is based on the result of the run with $E_0/B_0 = -0.04$ and $x_d/x_b = 0.42$. Figure 2 shows the temporal evolution of the profiles of out-of-plane electric field $-E_z$, current density $-j_z$, electron density n_e, ion out-of-plane flow velocity $-u_{iz}$, and ion temperature T_i along the y axis, where E_z is normalized by B_0. The reconnection electric field defined as E_z at the X point is a direct measure of the reconnection rate. The reconnection electric field begins to grow slowly as soon as both the plasma density and the current density increase in the current layer through the compression driven by plasma inflow from the upstream boundary ($y = \pm 64\lambda_{d0}$). When the plasma density is compressed to approach its peak values at $\omega_{ci0}t \sim 4.5$, magnetic reconnection sets in near the center. Then the reconnection field rapidly grows up. Consequently, the generation of the outflow away from the X point causes the density decrease in the vicinity of the X point, while the current density continues to increase. The reconnection field starts to saturate at $\omega_{ci0}t \sim 6$ when the current layer is compressed to approach the electron characteristic scale, l_{me} or c/ω_{pe}, where l_{me} is the electron meandering orbit amplitude. The meandering orbit amplitude of species s is given by $l_{ms} = \rho_s(l_{ms})$, where $\rho_s(y) = v_{ts}/\omega_{cs}$ is the local Larmor radius associated with B_x, and $v_{ts} = \sqrt{T_s/m_s}$ is the thermal velocity. As time goes on, the reconnection process gradually relaxes toward a steady state in which all the profiles shown in Fig. 2 are almost kept unchanged with time. The steady reconnection rate is mainly controlled by the external driving electric field E_0 ($= -0.04B_0$), which is consistent with the requirement for a 2D steady state. According to Faraday's law, the out-of-plane electric field becomes uniform in space and constant in time, and thus must be equal to the external driving field E_0 at the boundary [see Fig. 2(a), though there is a small fluctuation around E_0].

Figure 2(b) shows that the current layer shrinks to the electron scale in the growing phase, and then relaxes to the ion-meandering orbit amplitude l_{mi}. Correspondingly, the plasma density changes from a single peak structure into a two-peak structure [see Fig. 2(c)]. The half-width of current layer d_{jz} and the density scale d_h are shown in Fig. 3, in which the electron orbit amplitude l_{me}, the ion orbit amplitude l_{mi}, and the electron skin depth δ_e are also plotted. Here the density scale is defined as the half-width for the case of the single-peak profile of density or the half peak-to-peak distance for the two-peak profile. It is seen that both current layer and electron density scales almost change with the same rate at all times, and approach l_{mi} in the steady state. This feature suggests that the structure of

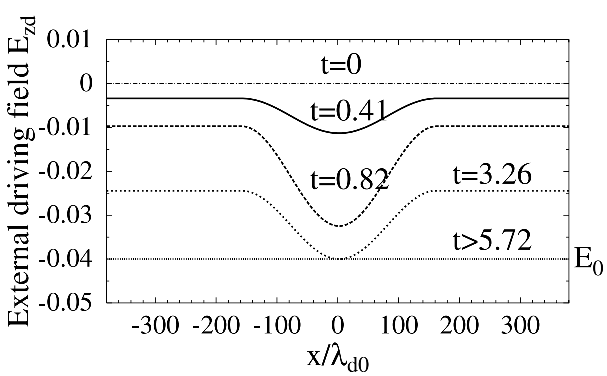

FIG. 1. The spatial profiles of the external driving electric field E_{zd} at the upstream boundary at 5 times normalized by ω_{ci0}^{-1} for $E_0 = -0.04B_0$ and $x_d/x_b = 0.42$.

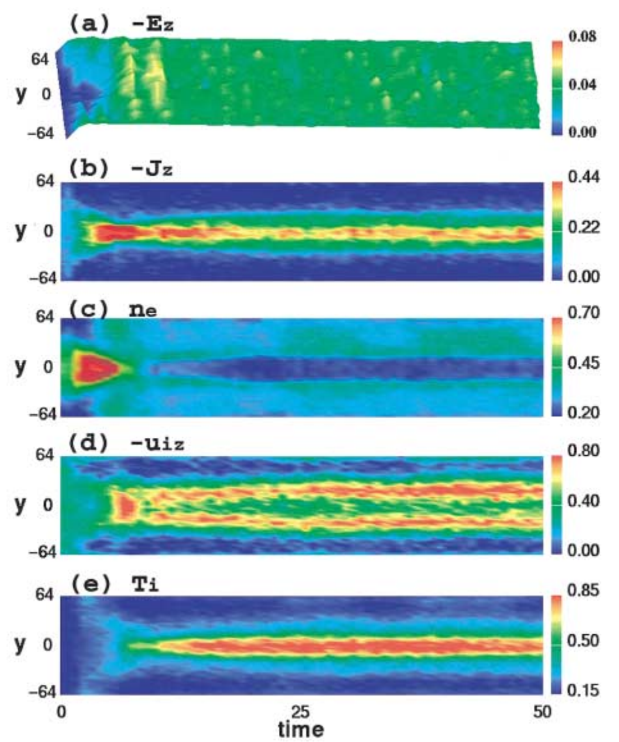

FIG. 2 (color). The temporal evolution of the profiles of out-of-plane electric field $-E_z$, current density $-j_z$, electron density n_e, ion out-of-plane flow velocity $-u_{iz}$, and ion temperature T_i along the y axis, where E_z normalized by B_0 is perspectively plotted and the time unit is ω_{ci0}^{-1}.

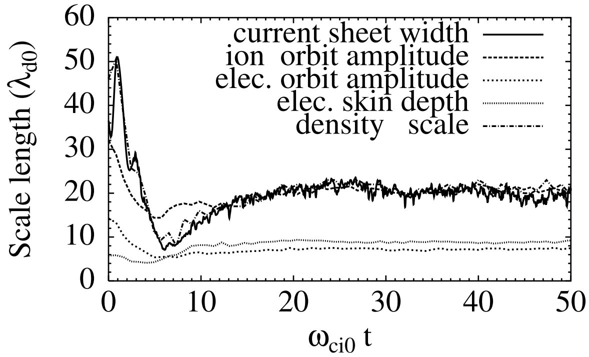

FIG. 3. The temperature evolutions of five spatial scales.

the current layer is modified by the plasma density configuration although the electron out-of-plane flow velocity is much higher in the reconnection region. The fact that the electron density is of ion orbit scale l_{mi} implies that the density is controlled by ion motion through the electrostatic interaction between ions and electrons. The steady ion out-of-plane flow exhibits a two-peak structure where the peak-to-peak distance is about $2l_{mi}$ [see Fig. 2(d)]. Similarly, the steady ion temperature T_i is strongly peaked on the x axis with the width of $2l_{mi}$ shown in Fig. 2(e). The profiles of n_e, u_{iz}, and T_i with the ion scale l_{mi} stretch out to the downstream boundary. In contrast, the electron temperature T_e is almost unchanged in the reconnection region (see Fig. 4).

Figure 4 shows the spatial profiles of electron and ion out-of-plane flow velocities u_{ez} and u_{iz}, the electric drift velocity $-cE_y/B_x$, and the electron thermal velocity v_{te} along the vertical line passing the X point ($x = x_r$), which are normalized by the initial electron thermal velocity v_{te0}. It is evident that the dissipation region has a two-scale structure underlying the quite different characteristic scale lengths of electron and ion dynamics. The ion motion decouples from the magnetic field due to the inertia effect within a region of $|y| \leq c/\omega_{pi}$ ($\simeq 40\lambda_{d0} \simeq 2l_{mi}$), while the electrons remain frozen in the magnetic field until they enter a region of scale c/ω_{pe} which is slightly larger than l_{me}.

Although the ion inertia is responsible for breaking the frozen-in constraint, the fact that the spatial structures of ion quantities have the scale l_{mi} implies that the ion-meandering motion plays an important role in ion dynamics. The two-peak structure in ion flow component $-u_{iz}$ is the typical consequence of ion-meandering motion in which the ions bounce back and forth across the x axis in the y direction with the average amplitude l_{mi} and have the maximum velocity component v_{iz} at the turning point. Because of the different motions between electrons and ions, an electrostatic field E_y is produced in the inflow direction. This field E_y dominates over the restoring force of ion bounce motion $u_{iz}B_x$ (see Fig. 4), and thus greatly intensifies the bounce frequency and energy. As a result, the meandering ions have the maximum values of velocity component v_{iy} on the x axis though the ion flow component u_{iy} vanishes there. Thus, the ion velocity distribution function at the X point exhibits two counterstreaming components in v_{iy} space, as shown in Fig. 5(a). Here v_y is normalized by $v_{tiy} = \sqrt{T_{iy}/m_i}$, and $T_{iy} = m_i\langle(v_y - u_{iy})^2\rangle$ is the ion temperature in the y direction. Similar results were presented in the hybrid simulations of magnetic reconnection [14]. This picture implies that ion heating is deeply related to the bounce motion because it does not contribute to the fluid kinetic energy. Figure 5(b) shows the spatial profiles of effective ion temperature T_i and three components T_{ix}, T_{iy}, and T_{iz} along the line $x = x_r$. The

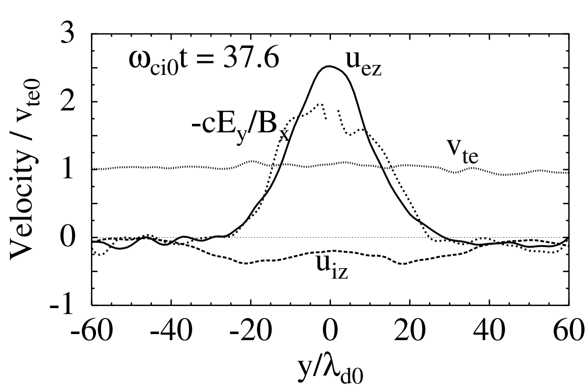

FIG. 4. The profiles of the out-of-plane velocities of electron flow u_{ez} and ion flow u_{iz}, the drift velocity $-cE_y/B_z$, and the electron thermal velocity v_{te} along the line $x = x_r$.

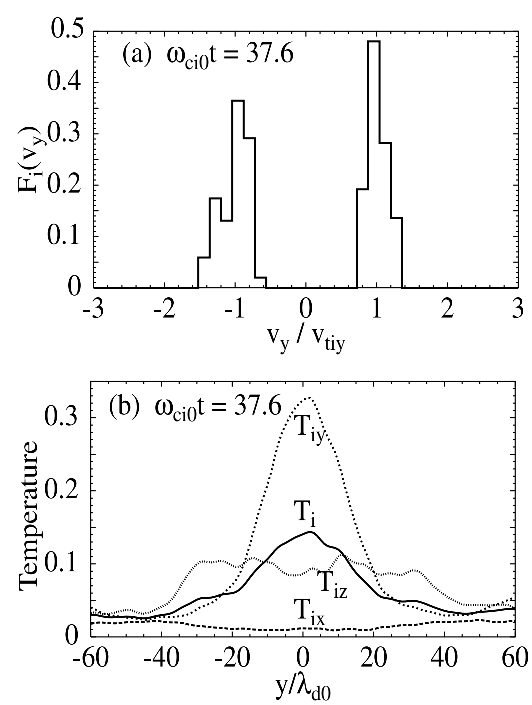

FIG. 5. (a) The ion velocity distribution function $f(v_{iy})$ at the X point, and (b) the profiles of the effective ion temperature T_i and three components T_{ix}, T_{iy}, and T_{iz} along the line $x = x_r$.

temperature T_{iy} in the y direction is much higher than those in the other directions in the region of $2l_{mi}$. Thus, the effective ion temperature T_i is peaked around the x axis with a scale of l_{mi}. This is mainly due to the work done by the electrostatic field E_y through the ion bounce motion.

The formation of the low-density channel with the width of $2l_{mi}$ is also due to the ion-meandering motion. The transit time for a meandering ion to pass the same distance in the y direction is longer near the turning point than near the neutral line. The difference of the transit times directly results in the density difference at two points. That is, the ion density at the turning point is larger than at the neutral line. This is the reason why the density channel can be formed in this region [see Fig. 2(c)].

The electrostatic field also has an effect on the electron dynamics. In contrast to the unmagnetized ions, the electrons are forced to drift with the velocity cE_y/B_x in the out-of-plane direction. Therefore, the electron flow gets a high velocity in the z direction before entering its dissipation region (Fig. 4). This is the reason why the current profile has the spatial scale of l_{mi}. In addition, since the electrostatic force cancels a large part of the restoring force of electron bounce motion, electron heating hardly occurs in the electron dissipation region.

In conclusion, the steady reconnection rate is mainly controlled by the driving electric field strength E_0. The dissipation region has a two-scales structure underlying the quite different characteristic scales of electron and ion dynamics. The electron frozen-in condition is broken mainly by an electron inertia. The ion inertia is responsible for the breaking of the ion frozen-in constraint, but the ion-meandering motion plays an important role in the ion dynamics which controls the spatial structures of plasma density, ion flow velocity, and ion temperature. Although the current is predominantly carried by electrons, the current layer has the half-width of the ion scale l_{mi} because the density profile is exclusively controlled by the massive ion motion. Thus, the global dynamical process of steady reconnection is dominantly controlled by ion dynamics. The electrostatic field generated through the finite Larmor radius effect is a key to coordinate the motions of electrons and ions. It leads to electron acceleration in the out-of-plane direction in the ion-dissipation region and ion heating by intensifying the meandering motion.

Our results are in good agreement with the recent experimental results in MRX [4,5] in the aspects of current layer width and ion heating. The current layer width $d_{jz} \approx l_{mi} \approx 0.5c/\omega_{pi}$ in this work is very close to the measurement value, $0.4c/\omega_{pi}$. We give a reasonable mechanism of ion heating; that is, ions are heated by the electrostatic field through the ion-meandering motion.

Numerical computations in this study are performed on the NIFS MISSION System (Grand Man-Machine Interactive System for Simulation).

[1] K. Schindler, J. Geophys. Res. **79**, 2803 (1974).

[2] V. M. Vasyliunas, Rev. Geophys. **13**, 303 (1975).

[3] A. M. Edwards *et al.,* Phys. Rev. Lett. **57**, 210 (1986).

[4] M. Yamada, H. Ji, S. Hsu, T. Carter, R. Kulsrud, and F. Trintchouk, Phys. Plasmas **7**, 1781 (2000).

[5] S. C. Hsu, G. Fiksel, T. A. Carter, H. Ji, R. M. Kulsrud, and M. Yamada, Phys. Rev. Lett. **84**, 3859 (2000).

[6] D. Biskamp, E. Schwarz, and J. F. Drake, Phys. Rev. Lett. **75**, 3850 (1995).

[7] M. Hesse, K. Schindler, J. Birn, and M. Kuznetsova, Phys. Plasmas **6**, 1781 (1999).

[8] M. A. Shay, J. F. Drake, and B. N. Rogers, Geophys. Res. Lett. **26**, 2163 (1999).

[9] T. Sato and T. Hayashi, Phys. Fluids **22**, 1189 (1979).

[10] R. Horiuchi and T. Sato, Phys. Plasmas **1**, 3587 (1994).

[11] R. Horiuchi and T. Sato, Phys. Plasmas **4**, 277 (1997).

[12] W. Pei, R. Horiuchi, and T. Sato, Phys. Plasmas **8**, 3251 (2001).

[13] R. Horiuchi, W. Pei, and T. Sato, Earth, Planets and Space **53**, 439 (2001).

[14] M. A. Shay, J. F. Drake, R. E. Denton, and D. Biskamp, J. Geophys. Res. **103**, 9165 (1998).